Supplement of Atmos. Chem. Phys., 20, 11955–11977, 2020
https://doi.org/10.5194/acp-20-11955-2020-supplement

Atmospheric Chemistry and Physics
Open Access
EGU

Supplement of

Accelerated increases in global and Asian summer monsoon precipitation from future aerosol reductions

Laura J. Wilcox et al.

Correspondence to: Laura Wilcox (l.j.wilcox@reading.ac.uk)

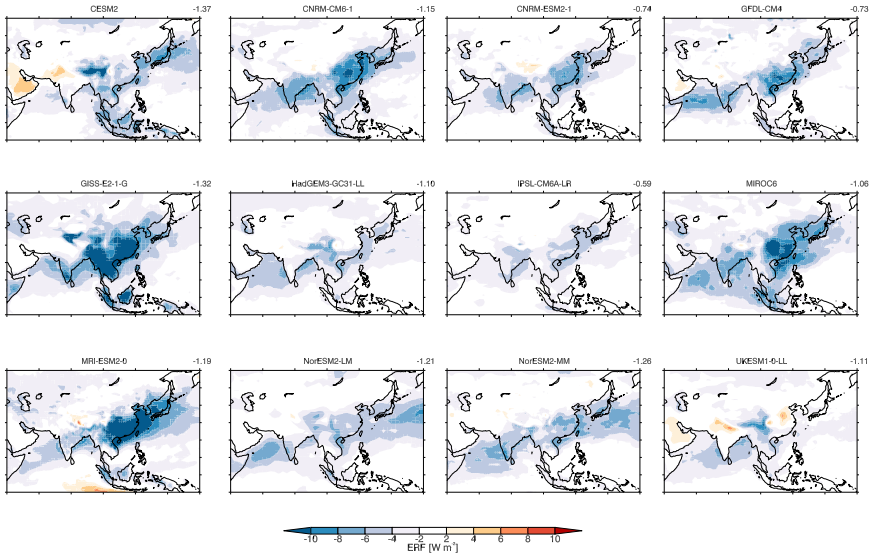

Figure S1. 2014 vs. 1850 effective radiative forcing (ERF) due to anthropogenic aerosols in individual CMIP6 models. The global mean value (in W m^{-2}) is shown in the top right of each panel. Figures S1 to S4 show the ERF due to different drivers, using the same colour scale. Model positions are consistent across the figures.

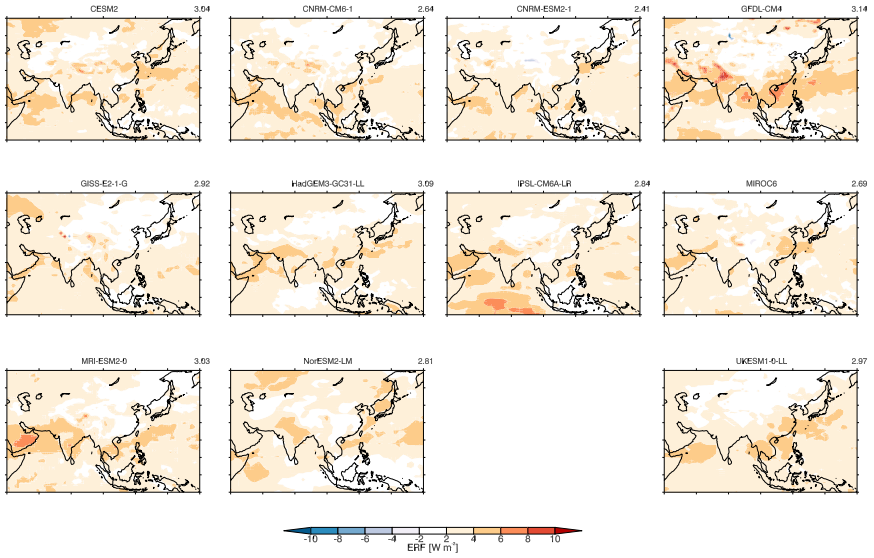

Figure S2. 2014 vs. 1850 effective radiative forcing (ERF) due to greenhouse gases in individual CMIP6 models. The global mean value (in W m^{-2}) is shown in the top right of each panel. Figures S1 to S4 show the ERF due to different drivers, using the same colour scale. Model positions are consistent across the figures.

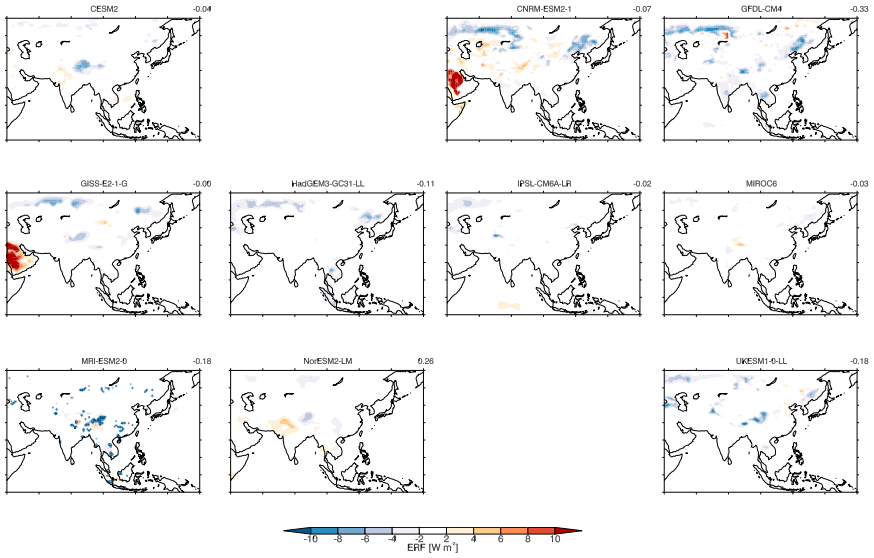

Figure S3. 2014 vs. 1850 effective radiative forcing (ERF) due to land use and land cover changes in individual CMIP6 models. The global mean value (in W m^{-2}) is shown in the top right of each panel. Figures S1 to S4 show the ERF due to different drivers, using the same colour scale. Model positions are consistent across the figures.

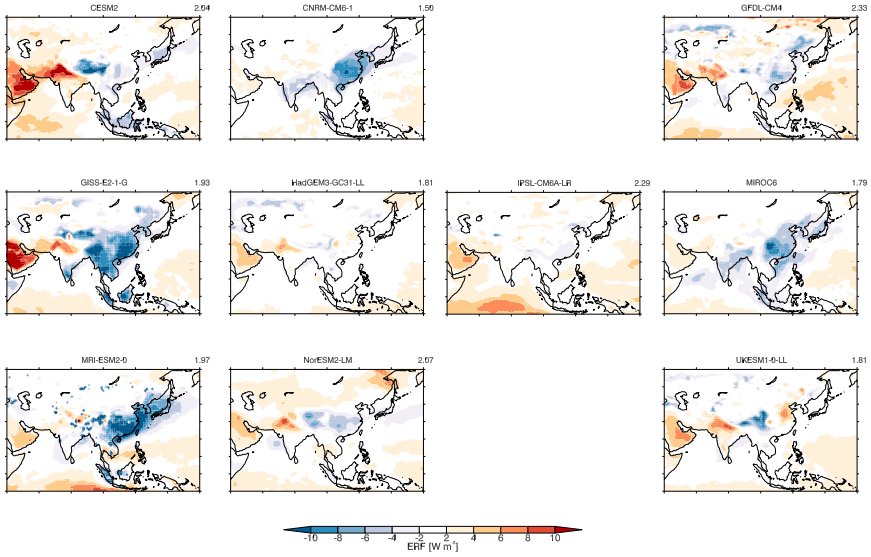

Figure S4. 2014 vs. 1850 effective radiative forcing (ERF) due to anthropogenic drivers in individual CMIP6 models. The global mean value (in W m^{-2}) is shown in the top right of each panel. Figures S1 to S4 show the ERF due to different drivers, using the same colour scale. Model positions are consistent across the figures.

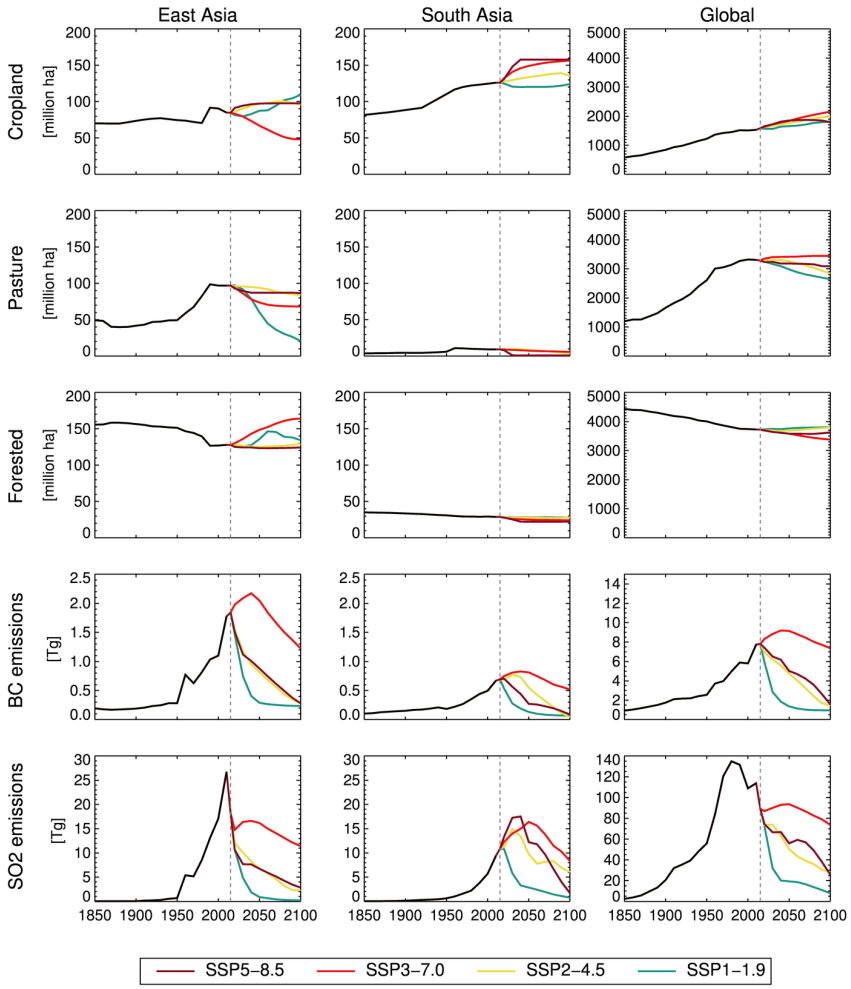

Figure S5. East Asian, South Asian, and global mean land use, and aerosol and precursor emissions from 1850 to 2100. The black line shows the historical period, and the coloured lines show the SSPs. For land use, 'cropland' is a sum of all c3 and c4 crop types, 'pasture' includes both managed and rangeland, and 'forested' is a sum of primary and secondary and secondary land.

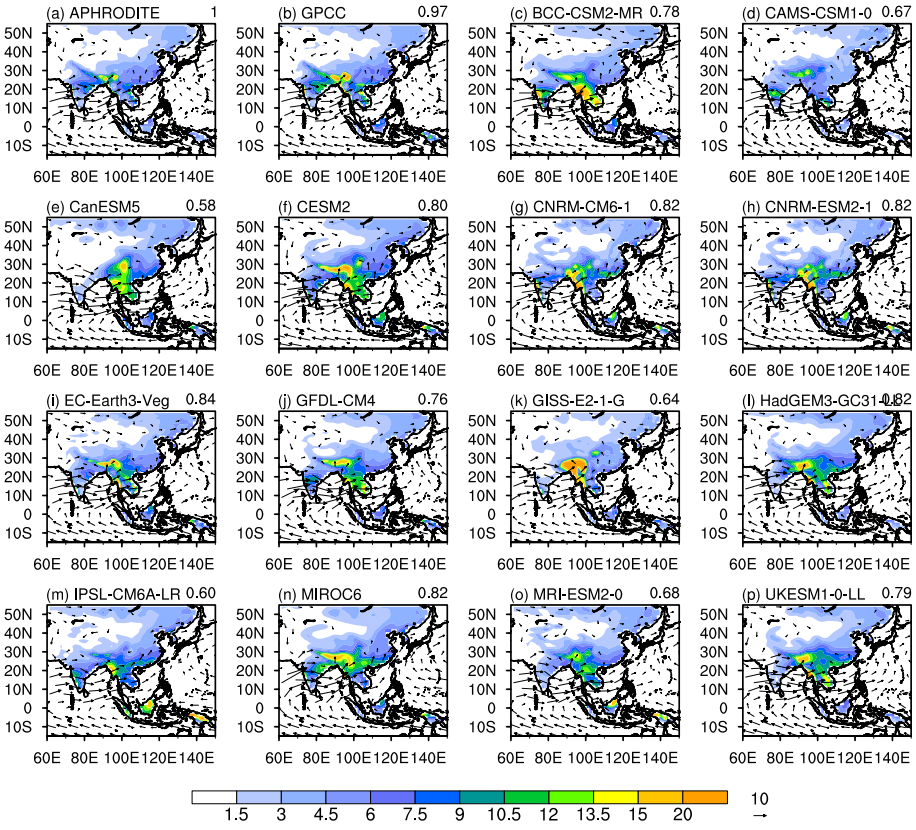

Figure S6. 1980-2014 JJA-mean precipitation [mm day^{-1}] and 850hPa winds [m s^{-1}] from (a): APHRODITE and ERA-Interim; (b): GPCC and ERA-Interim; (c)-(p): Individual CMIP6 models. Values in the top right corner of each panel show the pattern correlation with APHRODITE precipitation.

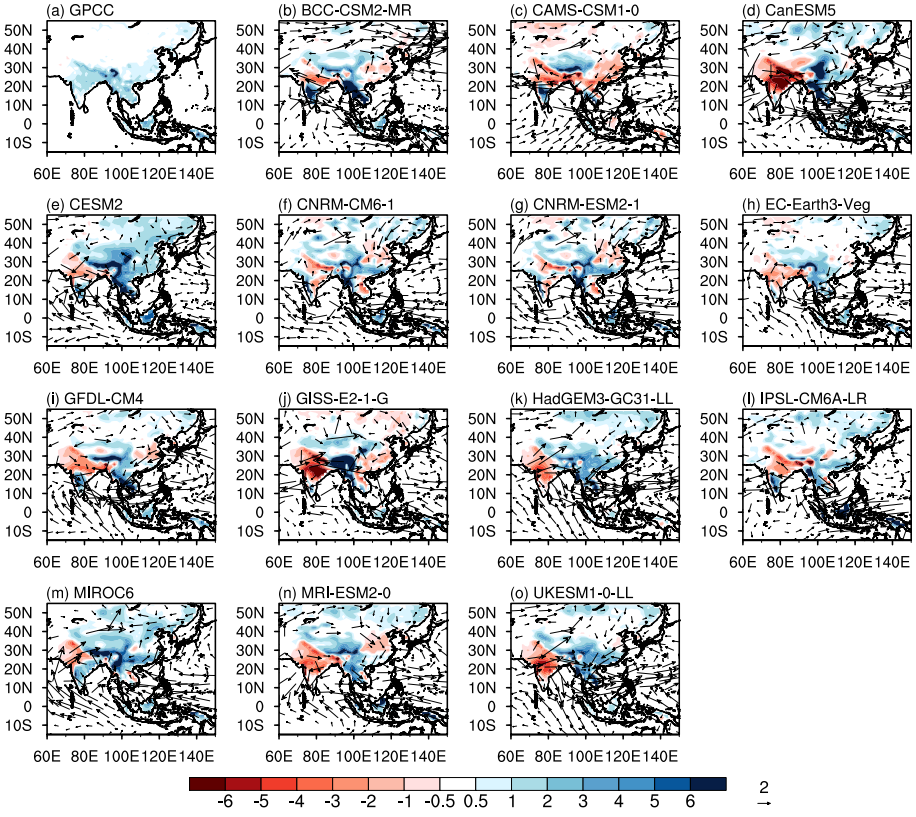

Figure S7. 1980-2014 JJA-mean precipitation relative to APHRODITE [mm day^{-1}] and 850hPa winds relative to ERA-Interim [m s^{-1}] from (a): GPCC and ERA-Interim; (b)-(o): Individual CMIP6 models.

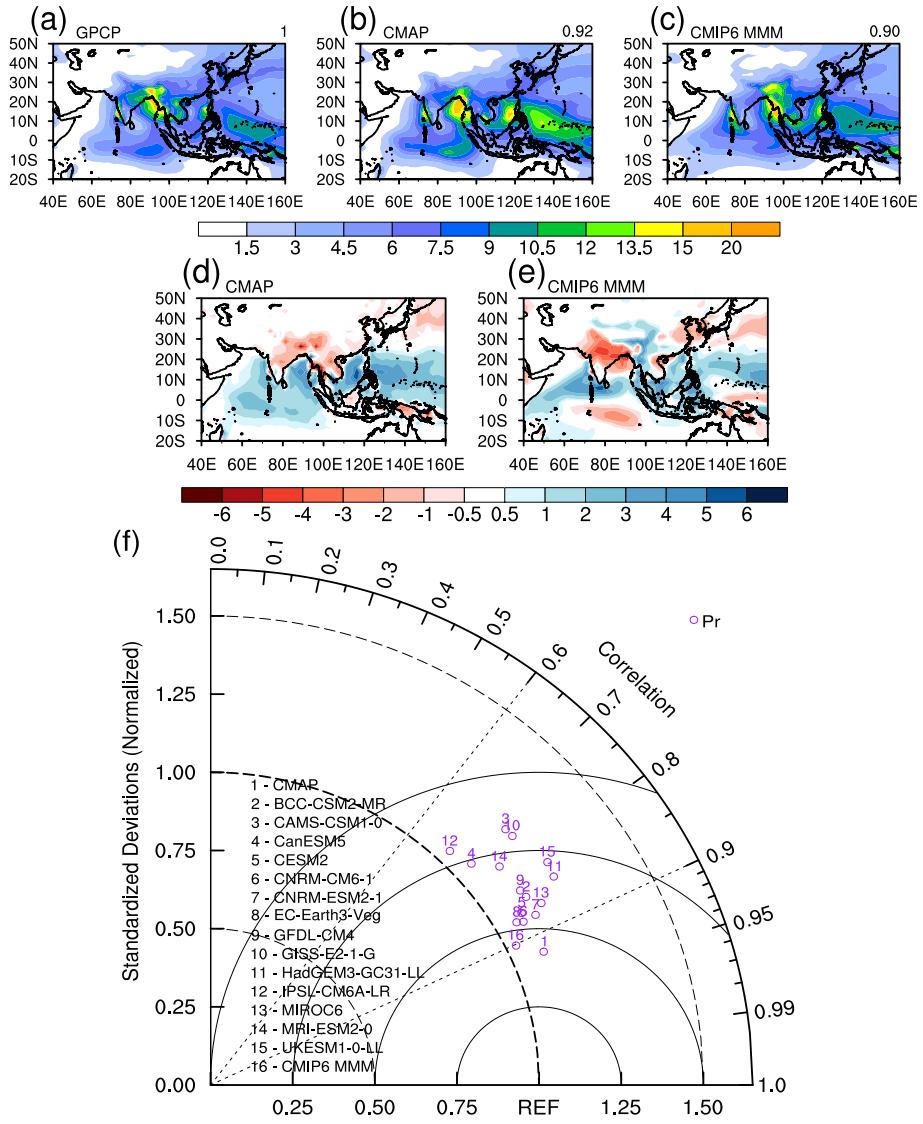

Figure S8. JJA-mean 1980-2014 mean precipitation overlaid with 850 hPa wind from (a): GPCP and ERA-Interim; (b): CMAP and ERA-Interim; (c): CMIP6 (multi-model mean). Values in the top right corner show the pattern correlation with APHRODITE precipitation. (d): Precipitation bias in CMAP relative to GPCP; (e): CMIP6 precipitation relative to GPCP and CMIP6 850 hPa winds relative to ERA-Interim. (f): Taylor diagram showing the relationship between individual CMIP6 models, the CMIP6 multi-model mean (point 16), and CMAP (point 1), with GPCC precipitation.

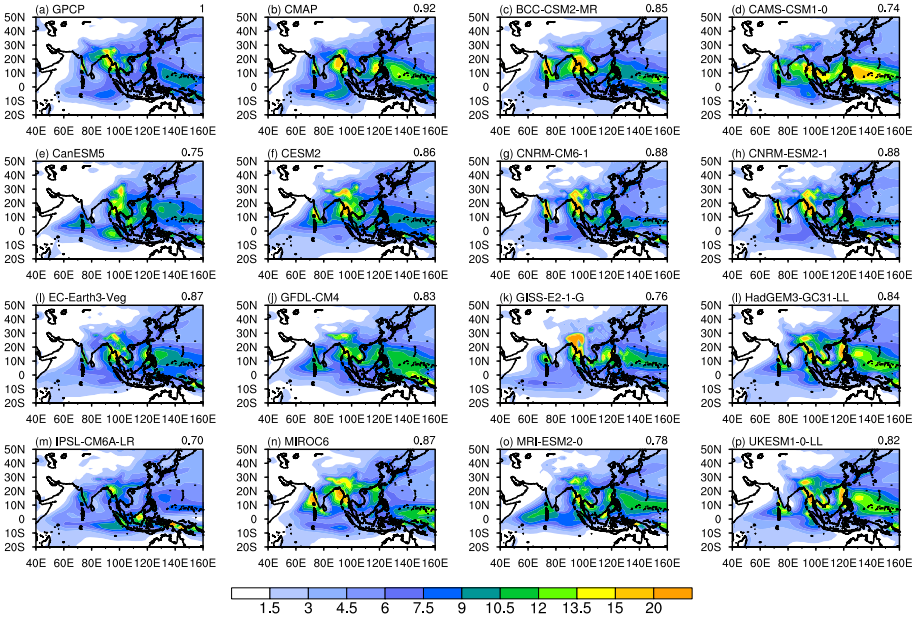

Figure S9. 1980-2014 JJA-mean precipitation [mm day^{-1}] from (a): GPCP; (b): CMAP; (c)-(p): Individual CMIP6 models. Values in the top right corner of each panel show the pattern correlation with GPCP precipitation.

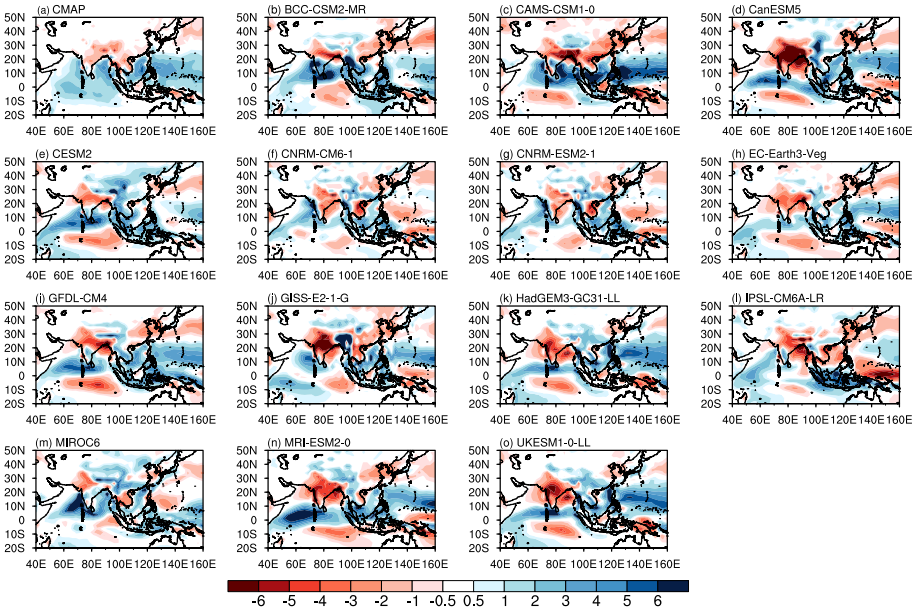

Figure S10. 1980-2014 JJA-mean precipitation [mm day^{-1}] relative to GPCP from (a): CMAP; (b)-(o): Individual CMIP6 models.

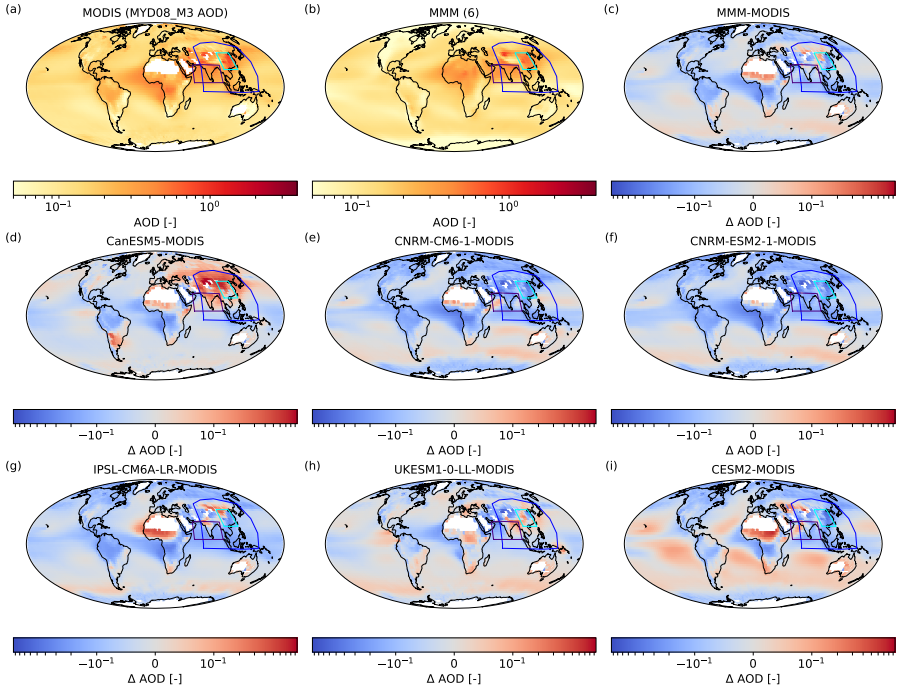

Figure S11. (a): 2002-2014 mean aerosol optical depth at 550 nm from MODIS; (b): 2002-2014 mean CMIP6 multi-model mean aerosol optical depth at 550 nm; (c): CMIP6 bias relative to MODIS, (d)-(i): Individual CMIP6 model biases relative to MODIS. Blue, purple, and turquoise boxes show the 'Asia', 'South Asia', and 'East Asia' regions used in later analysis.

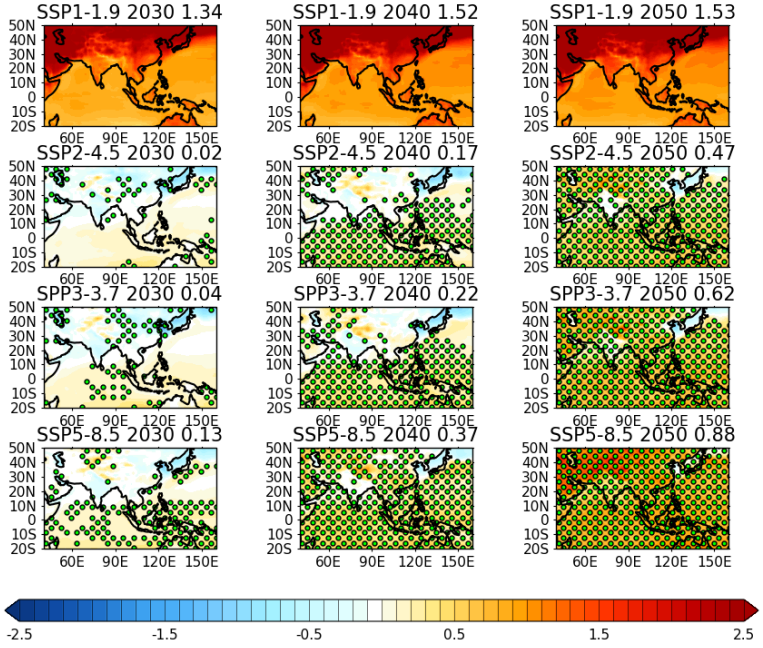

Figure S12. (a): CMIP6-mean JJA-mean near-surface temperature anomaly [K] for 2025-2034, 2035-2044, and 2045-2054 vs. 1980-2014 from SSP1-1.9. Relative anomalies for (b): SSP2-4.5.; (c): SSP3-7.0; and (d): SSP5-8.5 vs. SSP1-1.9. The numbers shown at the top right of each panel are the Asian mean, where Asia is the region bounded by 5-47.5°N, 67.5-145°E. Stippling shows where at least 70% of the models agree on the sign of the anomaly.

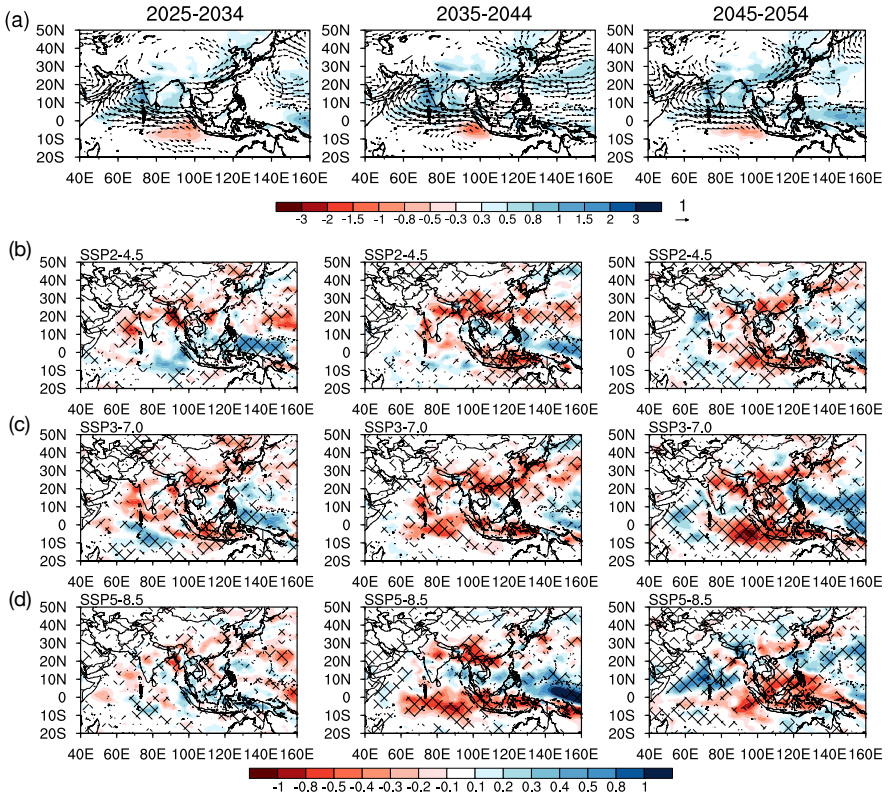

Figure S13. (a): JJA-mean precipitation [mm day^{-1}] for 2025-2034, 2035-2044, and 2045-2054 vs. 1980-2014 from SSP1-1.9. Anomalies from (b): SSP2-4.5; (c): SSP3-7.0; and (d): SSP5-8.5 relative to the anomalies from SSP1-1.9. Hatching shows where at least 70% of the models agree on the sign of the anomaly.

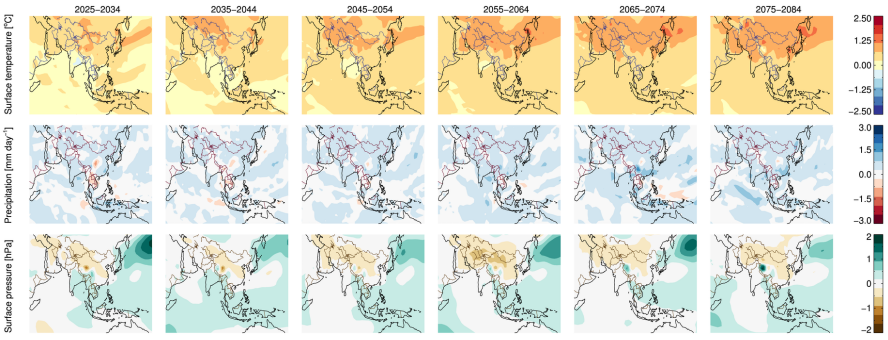

Figure S14. JJA (a): near-surface temperature [K]; (b): precipitation [mm day^{-1}]; and (c): sea level pressure [hPa] anomalies for 10 year periods vs. 1980-2014 from an anthropogenic aerosol only version of SSP2-4.5 (SSP2-4.5-aer) with CanESM5.

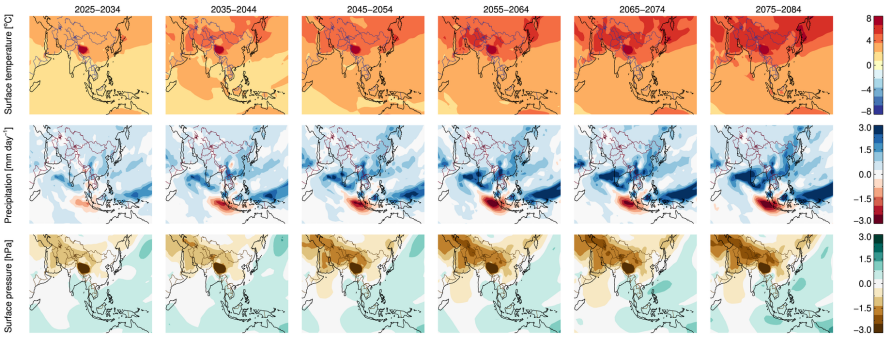

Figure S15. JJA (a): near-surface temperature [K]; (b): precipitation [mm day^{-1}]; and (c): sea level pressure [hPa] anomalies for 10 year periods vs. 1980-2014 from SSP2-4.5 with CanESM5.

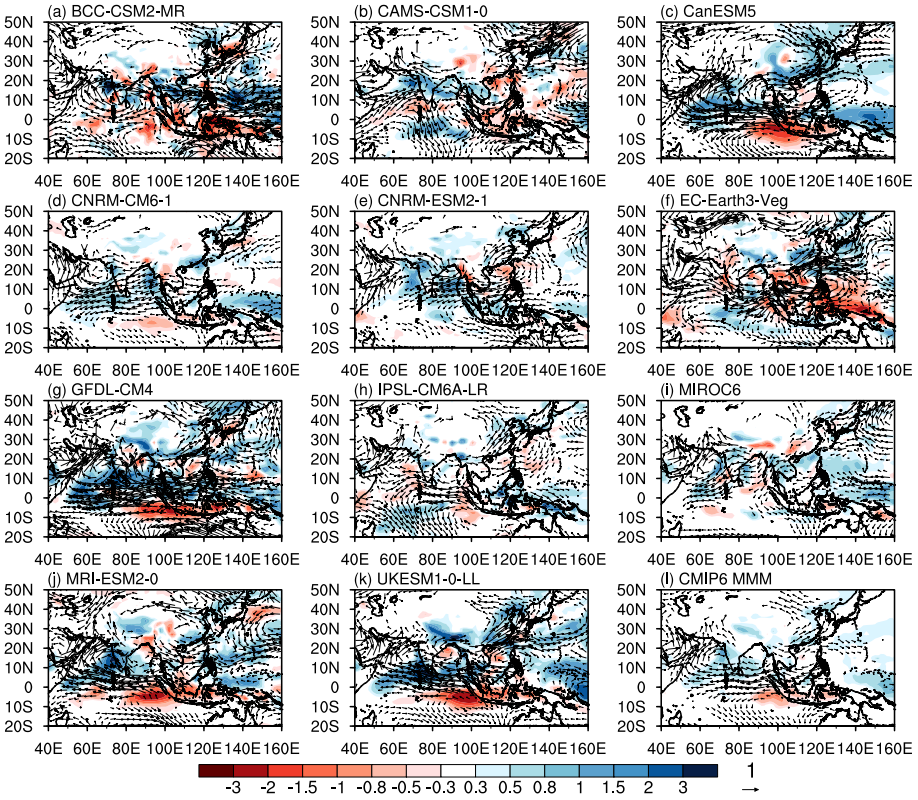

Figure S16. JJA precipitation [mm day^{-1}] and 850 hPa wind [m s^{-1}] anomalies for SSP2-4.5 2035-2044 vs. 1980-2014 for (a)-(l): Individual CMIP6 models; (m): The CMIP6 multi-model mean.